Electronic Supplementary Information (ESI)

Pre-synthetic strategy to construct single ion conductive covalent organic frameworks

Section 1. Methods

Characterization.

The powder X-ray diffraction (PXRD) data was carried out on a Rigaku model RINT Ultima III diffractometer by depositing powder on glass substrate, from 2θ=2° up to 40° with 0.02° increment. The N_2 adsorption-desorption isotherms were obtained on an ASAP2020 analyzer. Before measurement, samples were degassed under vacuum at 393 K for 6 h. Surface area of the samples was calculated by the Brunauer-Emmet-Teller (BET) method. Pore size distribution of the samples was analyzed by the Non-local-density functional theory (NLDFT). The ^{1}H-NMR spectra were recorded on a Bruker AVANCE IIITM 400 spectrometer (operating at 400 MHz). Thermogravimetric analysis (TGA) was determined on a Setaram Labsys Evo apparatus. The samples were heated in an alumina pan from 30 °C to 800 °C at a heating rate of 10 °C/min under argon atmosphere. Fourier transform infrared (FTIR) spectra were obtained using a Nicolet iS5 spectrophotometer (frequency range from 4000 to 500 cm^{-1}) with KBr pellet. The metal Li amount of Tp-PaSO_3Li-COF was determined by NexION 350 Inductively Coupled Plasma Optical Emission Spectrometer (ICP-OES). X-ray photoelectron spectroscopy (XPS) was employed on the PHI-5702 instrument and the C1s line at 284.5 eV was used as the binding energy reference. CHN analysis was performed using Vario MACRO Tube. Solid state ^{13}C MAS NMR spectroscopy was obtained on a Bruker AVANCE IIITM 600 MHz spectrometer using a 5 mm probe under magic-angle spinning.

Conductivity measurement.

Ion Conductivity measurements were performed on sample pellets using Solartron 1260 frequency response analyzer over a frequency range from 1 MHz to 0.1 Hz and with an input voltage amplitude of 10 mV. The sample pellets were tightly connected between two copper electrodes by means of spring, to ensure good contact between sample and each electrode.

Li-ion transference number(t_{Li+}).

The lithium-ion transference number of Tp-PaSO_3Li COF was measured using Li/Tp-PaSO_3Li-COF pellet/Li coin cells, where Tp-PaSO_3Li COF pellets were mounted between two lithium metal electrodes. The transference number t_{Li+} was evaluated by dc potentiostatic measurements in conjunction with Ac impedance spectroscopy according to the procedure described by Ghosh and Wang et al.[S2] Potentiostatic measurements were carried out to determine the initial I_0 and final steady-state I_{ss} currents by applying a dc polarization voltage of 10 mV across the samples. Impedance spectroscopy frequency range from 1

MHz to 1 Hz was used to determine the pellets' resistances (before R_o and after R_{ss}) the potentiostatic measurements. t_{Li+} were calculated according to the following equation:

$$t_{Li+} = \frac{I_s(\Delta V - I_0 R_0)}{I_0(\Delta V - I_{ss} R_{ss})}$$

where ΔV is the DC polarization voltage applied. A Solartron 1287/1260 electrochemical workstation was used to carry out the tests. The testing parameters were controlled by the associated CorrWare and ZPlot softwares, while the resulting data were analyzed using CorrView and ZView.

Computational calculations.

The crystalline structure of Tp-PaSO_3Li-COF was determined using density functional theory/local density approximation (DFT/LDA) in Castep module and pawley refinement was carried out using Reflex, a software package for crystal determination from XRD pattern, implemented in MS modeling version 4.4 (Accelrys Inc.). Initially, unit cell dimensions for both hexagonal and rhombic lattices were taken from the DFT calculation and the space group for hexagonal and rhombic crystal system were selected as P3(C3-1), respectively. Pawley refinement was performed for hexagonal lattice to optimize the lattice parameters iteratively until the R_{WP} value converges. The pseudo Voigt profile function was used for whole profile fitting and Berrar-Baldinozzi function was used for asymmetry correction during the refinement processes.

For theoretical calculations on migration of Li ion, DFT calculations were performed using DMol^3 program.[1] Generalized gradient approximation with Perdew-Burke-Ernzerhof functional (GGA-PBE)[2] was used for the exchange-correlation energy along with the double numerical polarization basis set. The SCF convergence for each electronic energy was set as 1.0×10^{-6} Ha, and the geometry optimization convergence criteria were set up as follows: 1.0×10^{-5} Ha for energy, 0.002 Ha Å^{-1} for force, and 0.005 Å for displacement, respectively. The parameters of unit cell structure and geometry were first optimized, which are found to be slightly less that from those of X-ray experiments (a=b=22.042 Å, c=5.149 Å, α=β=90., γ=120. vs. a=b=22.1843 Å, c=5.1666 Å, α=β=90., γ=120.). The 1×1×2 supercell model with one vacant site of Li^+ was used to study Li-ion migration, which were examined by linear and quadratic synchronous transit (LST/QST) methods in combination with the conjugated gradient (CG) refinements.

Battery tests.

Aluminium-coated $LiFePO_4$ active materials were used to formulate the composite cathode. The cathode electrode was prepared by homogenously blending $LiFePO_4$, acetylene black, and polyvinylidene fluoride (PVDF) with a ratio of 8:1:1 in NMP. A mixture of the components was casted onto a surface-

treated aluminium current collector. After drying in a vacuum oven at 60 ℃ for 12 h, a composite electrode was obtained. Finally, the batteries were assembled by combining a separate cathode, a separate solid electrolyte pellet and a metal lithium sheet into a CR2016 coin-type cell in glove box in Ar atmosphere. Batteries were cycled using a Land battery testing system, the potential window was 3.6 V to 2.5 V for regimes at 0.2C; The specific capacity is calculated based on the active materials in the cathode, which corresponds to an area loading of about 1.25 mg/cm^2. 1 C charge/discharge rate here is defined as 170 mAh/g.

Section2. Materials and Synthetic Procedures

Materials.

Phloroglucinol, hexamethylenetetramine, Trifluoroacetic acid, 2,5-Diaminobenzenesulfonic acid were purchased from TCI Reagent Co. Sodium hydroxide (NaOH), potassium hydroxide (KOH), lithium hydroxide (LiOH) were purchased from Aladdin Reagent Co. All other chemicals were of analytical grade and were used without any further purification.

Synthesis of Triformylphloroglucinol (Tp).

Triformylphloroglucinol (Tp) was prepared according to previous reported literature procedure. [S1] Hexamethylenetetramine (15.098 g, 108 mmol) and dried phloroglucinol (6.014 g, 49 mmol) under N_2 was added into 90 mL trifluoroacetic acid. The solution was heated and stirred at 100 ºC for ca. 2.5 h. Approximately 150 mL of 3 M HCl was added and the solution was heated at 100 ºC for 1 h. After cooling to room temperature, the solution was filtered through Celite, extracted with ca. 350 mL dichloromethane, dried over magnesium sulfate, and filtered. Rotary evaporation of the solution afforded an off-white powder, a pure sample was obtained by sublimation. ^{1}H NMR (300 MHz, DMSO-d6, δ): 10.69 (s, 3H, OH); 10.04 (s, 3H, CHO);

Synthesis of 2,5-Diaminobenzene-sulfonic lithium ($PaSO_3Li$).

2,5-Diaminobenzenesulfonic acid (0.188 g, 0.1 mol) was dispersed in 10 mL THF and protected with N_2. Then LiOH (0.024 g, 0.1 mol) was added. The solution was stirred at room temperature for 4 h. The mixture will then turn into a clear dark purple solution. Then the solvent was removed under vacuum. The final product $PaSO_3Li$ was then dried under vacuum. ^{1}H NMR (400 MHz, DMSO-d6, δ): 6.84 (s, 1 H, ArH); 6.34 ppm (s, 2 H, ArH); 4.62 (s, 4 H, NH_2).

Synthesis of 2,5-Diaminobenzene-sulfonic sodium ($PaSO_3Na$).

2,5-Diaminobenzenesulfonic acid (0.188 g, 0.1 mol) was dispersed in 10 mL THF and protected with N_2. Then NaOH (0.04 g, 0.1 mol) was added. The solution was stirred at room temperature for 4 h. The mixture will then turn into a clear dark purple solution. Then the solvent was removed under vacuum. The final product $PaSO_3Na$ was then dried under vacuum. ^{1}H NMR (400 MHz, DMSO-d6, δ): 6.96 (s, 1 H, ArH); 6.46 ppm (s, 2 H, ArH); 5.33 (s, 4 H, NH_2).

Synthesis of 2,5-Diaminobenzene-sulfonic potassium ($PaSO_3K$).

2,5-Diaminobenzenesulfonic acid (0.188 g, 0.1 mol) was dispersed in 10 mL THF and protected with N_2. Then KOH (0.04 g, 0.1 mol) was added. The solution was stirred at room temperature for 4 h. The mixture will then turn into a clear dark purple solution. Then the solvent was removed under vacuum. The final product $PaSO_3Na$ was then dried under vacuum. ^1H NMR (400 MHz, DMSO-d6, δ): 6.84 (s, 1 H, ArH); 6.34 ppm (s, 2 H, ArH); 4.62 (s, 4 H, NH_2).

Synthesis of Tp-$PaSO_3Li$-COF. A mixture of Mesitylene/Dioxane (0.8 mL/0.2 mL), $PaSO_3Li$ (25.3 mg, 1.35 mmol), Tp (18.94 mg, 0.9 mmol) and 50 μL acetic acid solution (0.1 M) was degassed in a 10 mL ampoule tube by three freeze-pump-thaw cycles. The tube was heated to 120 ºC for 3 days. The precipitate was collected by filtration, washed with H_2O and THF, and dried at 120 ºC under vacuum overnight t to give Tp-$PaSO_3Li$-COF in 80 % yield.

Synthesis of Tp-$PaSO_3Na$-COF. A mixture of Mesitylene/Dioxane (0.8 mL/0.2 mL), $PaSO_3Na$ (28.4 mg, 1.35 mmol), Tp (18.94 mg, 0.9 mmol) and 50 μL acetic acid solution (0.1 M) was degassed in a 10 mL ampoule tube by three freeze-pump-thaw cycles. The tube was heated to 120 ºC for 3 days. The precipitate was collected by filtration, washed with H_2O and THF, and dried at 120 ºC under vacuum overnight t to give Tp-$PaSO_3Na$-COF in 75 % yield.

Synthesis of Tp-$PaSO_3K$-COF. A mixture of Mesitylene/Dioxane (0.8 mL/0.2 mL), $PaSO_3K$ (30.5 mg, 1.35 mmol) and Tp (18.94 mg, 0.9 mmol), and 50 μL acetic acid solution (0.1 M) was degassed in a 10 mL ampoule tube by three freeze-pump-thaw cycles. The tube was heated to 120 ºC for 3 days. The precipitate was collected by filtration, washed with H_2O and THF, and dried at 120 ºC under vacuum overnight t to give Tp-$PaSO_3K$-COF in 76 % yield.

Section 3. Supporting Tables

Table S1. Atomistic coordinates for pawley-refined unit cell parameters of Tp-PaSO_3Li-COF optimized by using DFT method. Space group: P_3; a=b=22.5866 Å, c = 5.3421 Å. α =β=90°, and γ=120°.

Atom	*x/a*	*y/b*	*z/c*
H	0.50353	0.66242	0.79067
H	0.52025	0.35435	0.9515
H	0.65873	0.49546	0.95388
H	0.36207	0.52999	0.81285
H	0.46679	0.40552	1.0509
H	0.65823	0.59132	0.83692
H	0.59238	0.65474	0.78394
C	0.49229	0.56572	0.87502
C	0.4571	0.49618	0.95967
C	0.49411	0.46153	0.98555
C	0.74086	0.37738	0.95553
C	0.71149	0.30284	0.95424
C	0.57852	0.39048	0.95127
C	0.56478	0.49316	0.93374
C	0.60001	0.56311	0.86735
C	0.56396	0.59788	0.83879
C	0.25944	0.63114	0.71436
C	0.29751	0.70609	0.69446
C	0.39711	0.58768	0.78003
N	0.4635	0.60732	0.81264
N	0.60235	0.45872	0.9468
S	0.36626	0.44333	1.04388
O	0.25963	0.52579	0.66502
O	0.35867	0.38085	1.15437
O	0.35188	0.48628	0.21984
O	0.32793	0.4321	0.8056
Li	0.2971	0.46695	0.1693

Table S2. Elemental analysis results

Tp-PaSO$_3$Li-COF	C %	N %	H %
	39.8	7.1	3.38

Table S3. ICP-OES results of Tp-PaSO$_3$Li-COF

Tp-PaSO$_3$Li-COF	Li (wt%)
Before EIS test	2.0
After EIS test	2.0

Table S4. t_{Li^+} value of Tp-PaSO$_3$Li -COF

ΔV (V)	I_0 (μA)	I_{SS} (μA)	R_0 (Ω)	R_{ss} (Ω)
0.01	0.315	0.297	563.8	570.2

Table S5. Thermodynamic parameters (kcal mol^{-1}) at room temperature for structures in axial migration pathway.

	Entropy	**Enthalpy**	**Free_Energy**	**ΔG**
1	-431.687	-753.807	-625.100	0.0
2	-425.402	-753.712	-626.878	-1.78
3	-431.063	-754.366	-625.845	-0.75
1-2	-432.091	-752.693	-623.865	1.24
2-3	-428.790	-753.739	-625.895	-0.80
3-4	-427.800	-752.385	-624.836	0.26

Table S6. Thermodynamic parameters (kcal mol^{-1}) at room temperature for structures in planar migration pathway.

	Entropy	**Enthalpy**	**Free_Energy**	**ΔG**
5	-431.342	-753.969	-625.364	-0.26
6	-434.638	-753.519	-623.932	1.17
7	-428.271	-753.438	-625.749	-0.65
4-5	-426.945	-753.026	-625.732	-0.63
5-6	-434.971	-752.251	-622.564	2.54
6-7	-428.322	-751.881	-624.177	0.92

Table S7. Summary of the performance of single Li^+ MOFs, COFs, polymers and silicas reported.

Sample	σ (S cm^{-1})	T (K)	E_a (eV)	t_{Li+}	Ref
MOF-LiI	1.1×10^{-4}	298	0.24	0.34	*J. Am. Chem. Soc.* **2019**, *141*, 4422.
MIT-$LiBF_4$	4.8×10^{-4}	298	0.16	0.75	*J. Am. Chem. Soc.* **2017**, *139*, 13260.
ICOF-2	3.1×10^{-5}	298	0.24	0.80	*Angew. Chem. Int. Ed.* **2016**, *55*, 1737.
CF_3-Li-ImCOF	7.2×10^{-3}	298	0.10	0.81	*J. Am. Chem. Soc.* **2019**, *141*, 7518.
TpPa-SO_3Li	2.7×10^{-5}	298	0.18	0.91	*J. Am. Chem. Soc.* **2019**, *141*, 5880.
SLIC-600	3.3×10^{-6}	303	--	0.86	*Chem Electro Chem* **2019**, *6*, 2219.
PSsTFSI	1.3×10^{-4}	363	--	0.91	*Angew. Chem. Int. Ed.* **2016**, *55*, 2521.
Tp-PaSO_3Li-COF	3.0×10^{-3}	363	0.13	0.94	**This Work**

Section 4. Supporting Figures

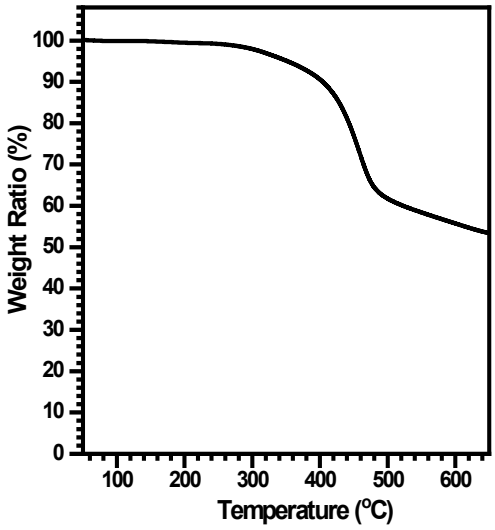

Figure S1. TGA curve of Tp-PaSO_3Li-COF

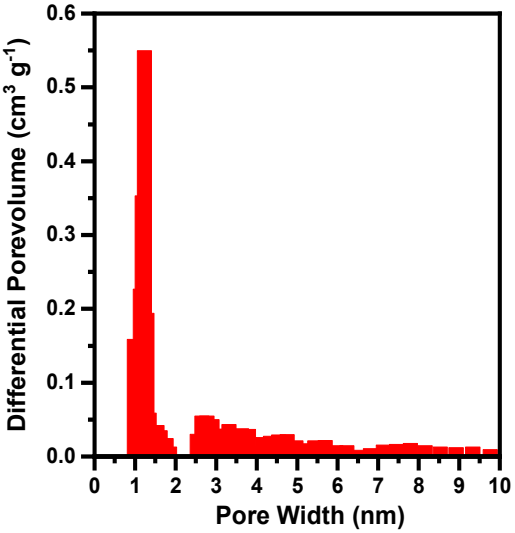

Figure S2. Pore size distribution of Tp-PaSO_3Li-COF

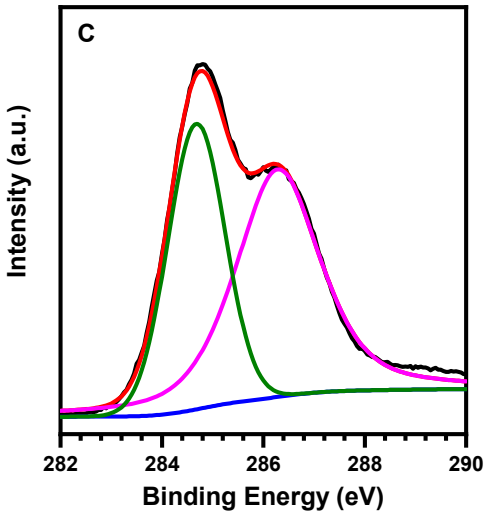

Figure S3. High-resolution XPS spectra of C 1s of Tp-PaSO_3H COF

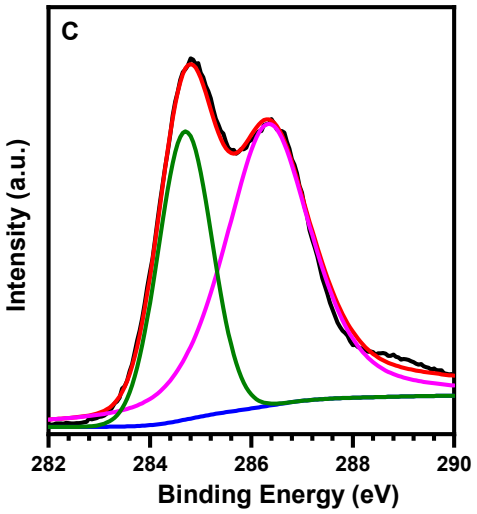

Figure S4. High-resolution XPS spectra of C 1s of Tp-PaSO_3Li-COF

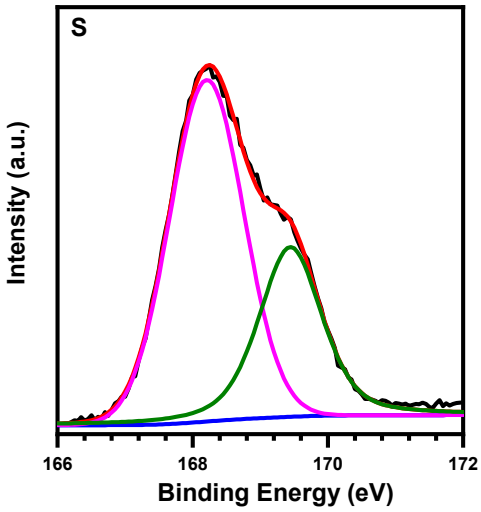

Figure S5. High-resolution XPS spectra of S2p of Tp-PaSO_3Li-COF

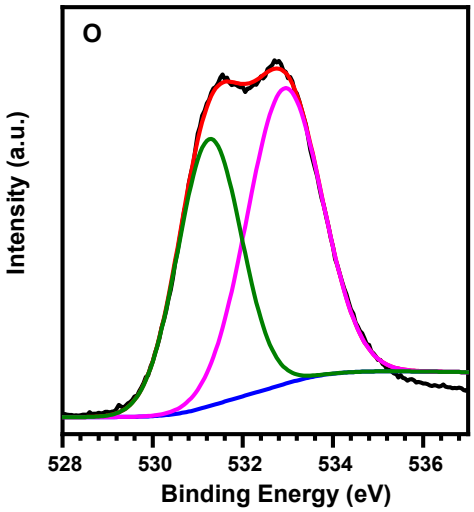

Figure S6. High-resolution XPS spectra of O 1s of Tp-PaSO_3H-COF

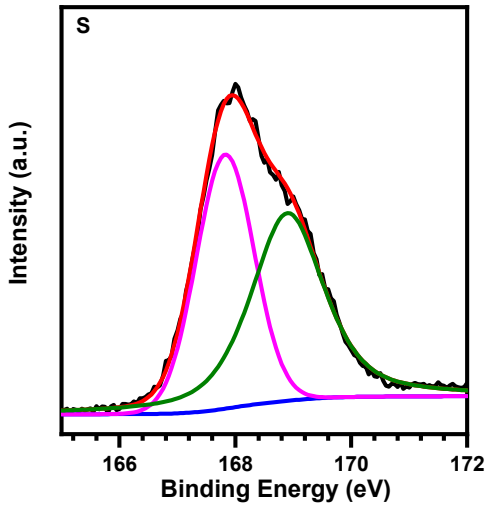

Figure S7. High-resolution XPS spectra of S 2p of Tp-PaSO_3H-COF

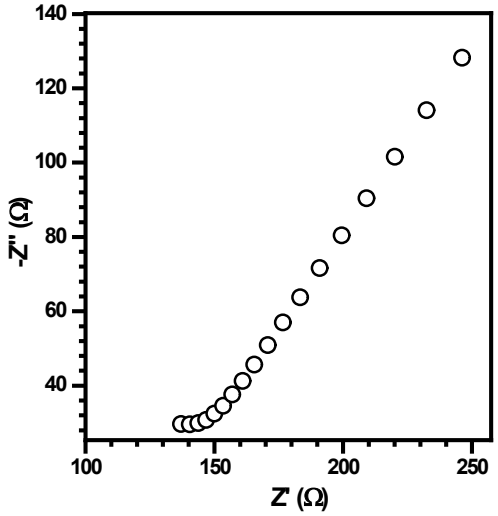

Figure S8. Nyquist plot of Tp-PaSO$_3$Li-COF at 293K

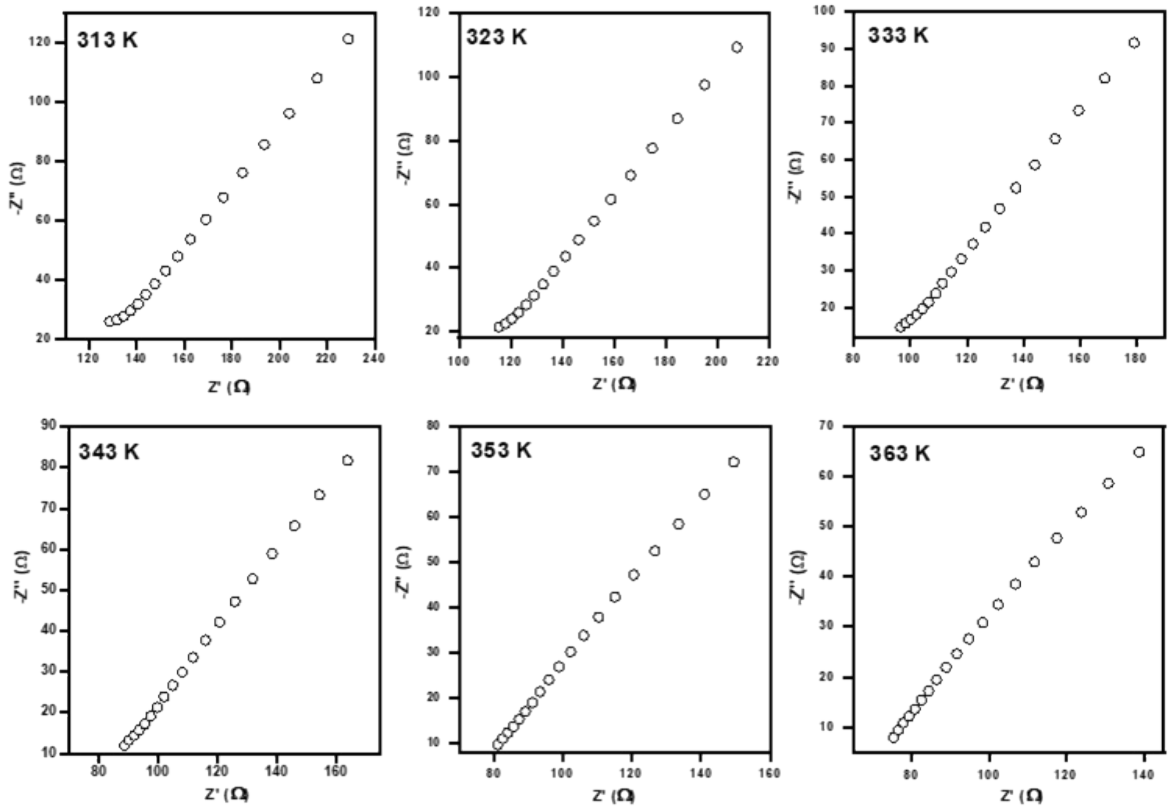

Figure S9. Nyquist plot of Tp-PaSO$_3$Li-COF at 313 K, 323 K, 333 K, 343 K, 353 K, 363 K respectively

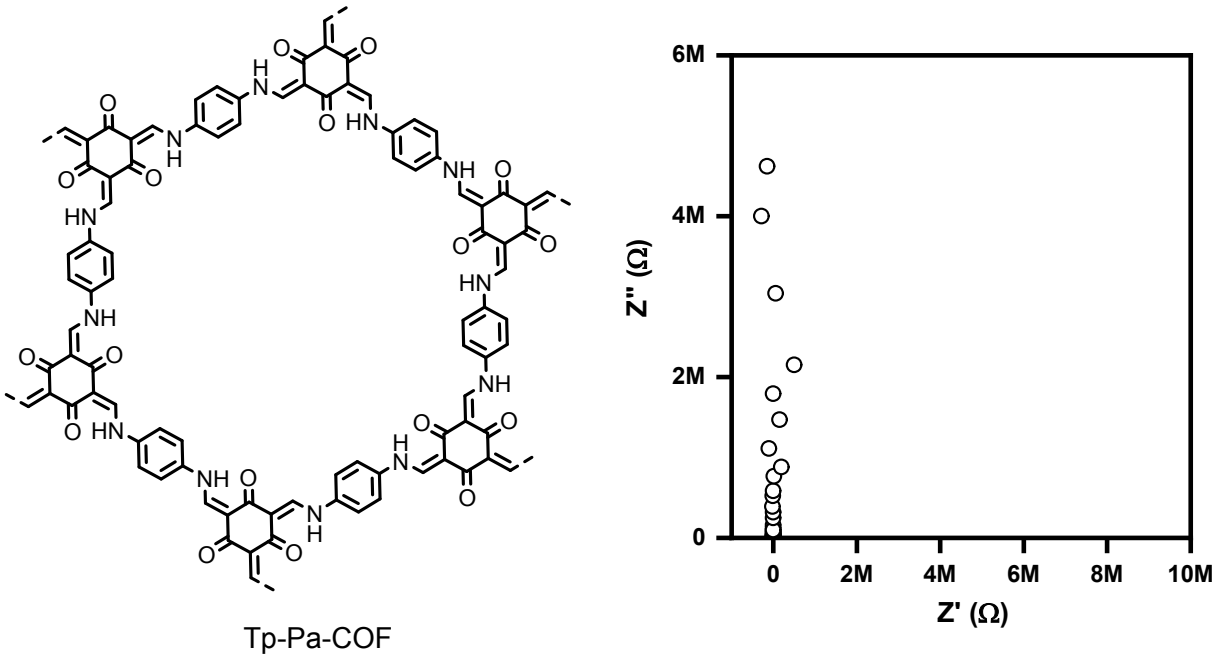

Figure S10. Nyquist plot of Tp-Pa-COF at 293 K

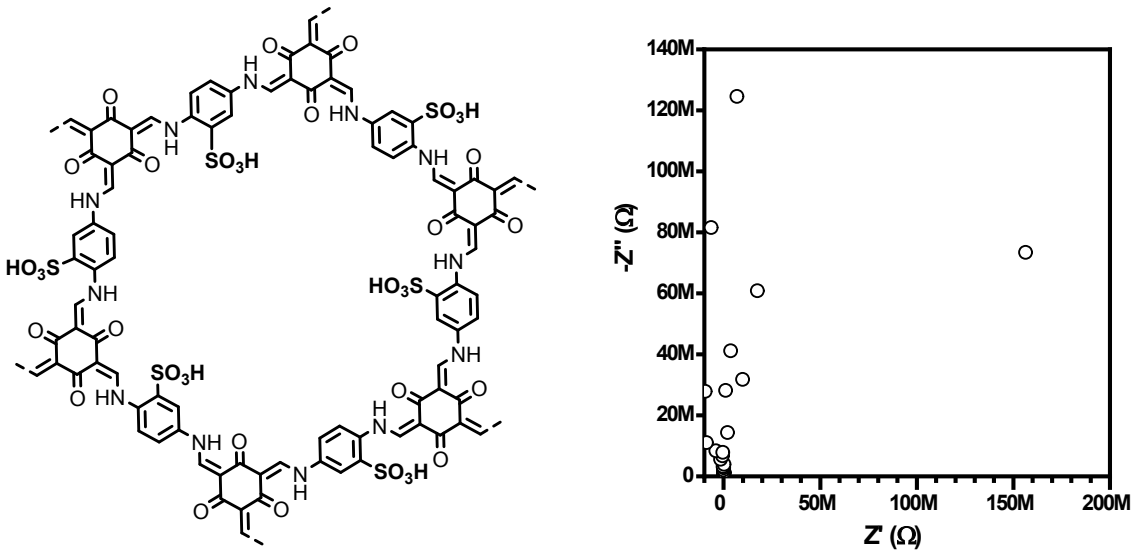

Figure S11. Nyquist plot of Tp-PaSO$_3$H-COF at 293 K

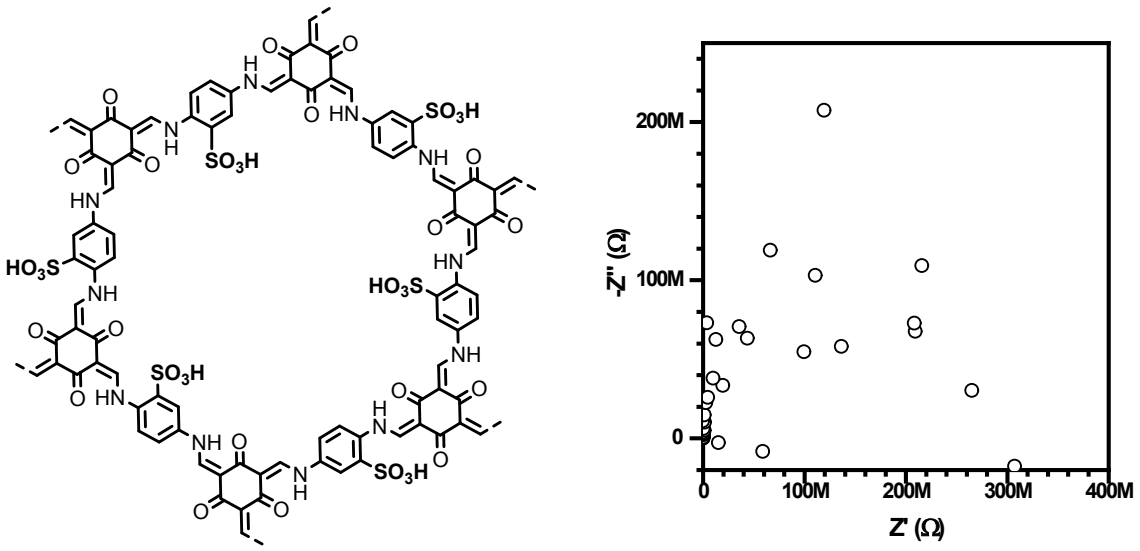

Figure S12. Nyquist plot of Tp-PaSO_3H-COF at 363 K

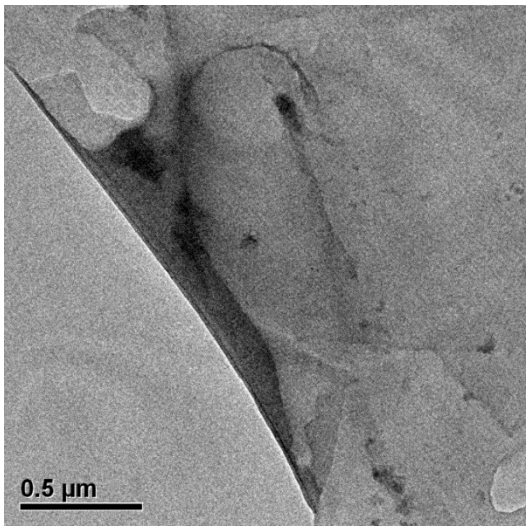

Figure S13. TEM morphology of Tp-PaSO_3Li-COF

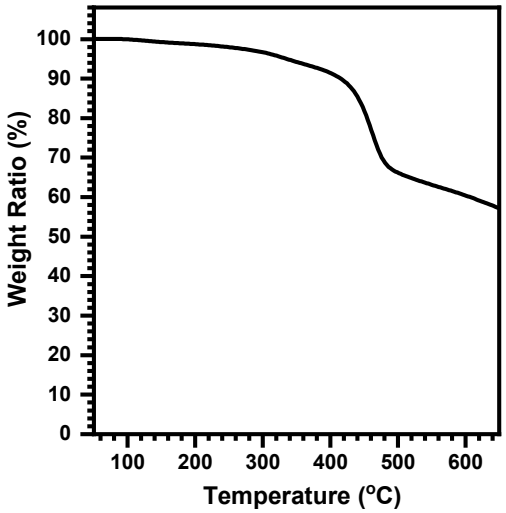

Figure S14. TGA curve of Tp-PaSO_3Na-COF

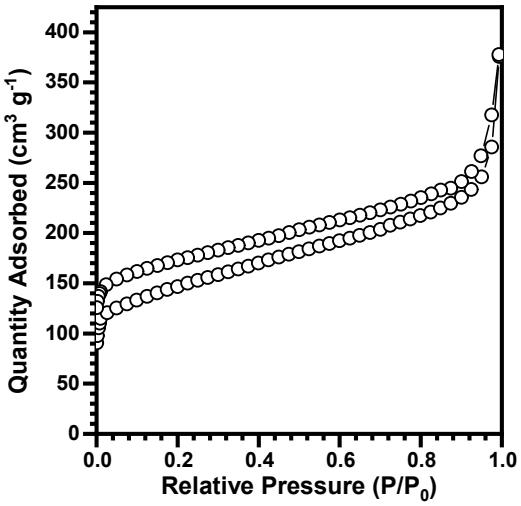

Figure S15. N_2 adsorption isotherm of Tp-PaSO_3Na-COF

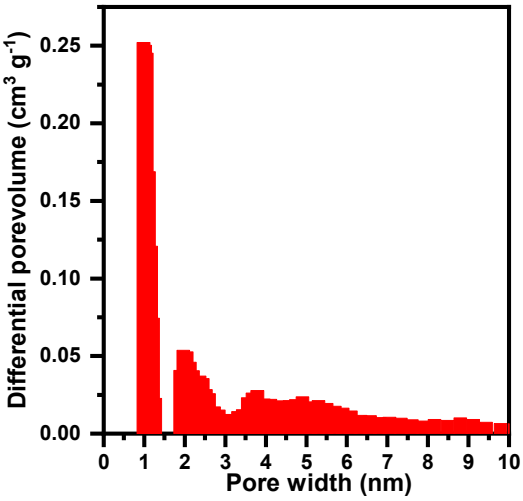

Figure S16. Pore size distribution of Tp-PaSO_3Na-COF

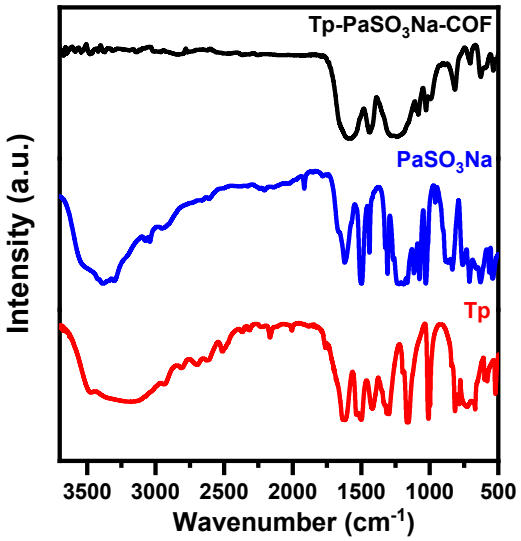

Figure S17. FT-IR spectra of $PaSO_3Na$, Tp and Tp-$PaSO_3Na$-COF

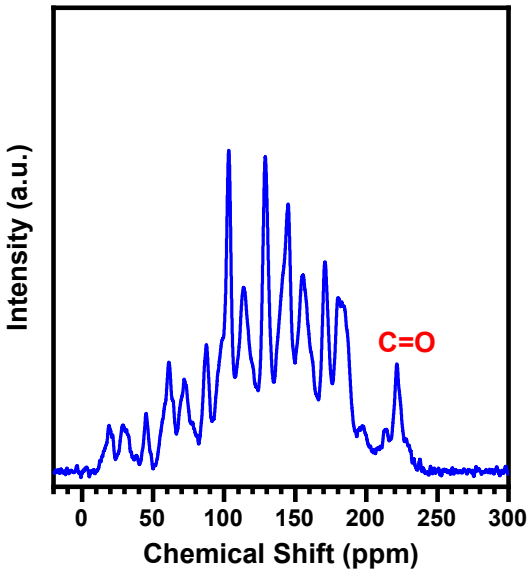

Figure S18. Solid state ^{13}C-NMR spectrum of Tp-PaSO$_3$Na-COF

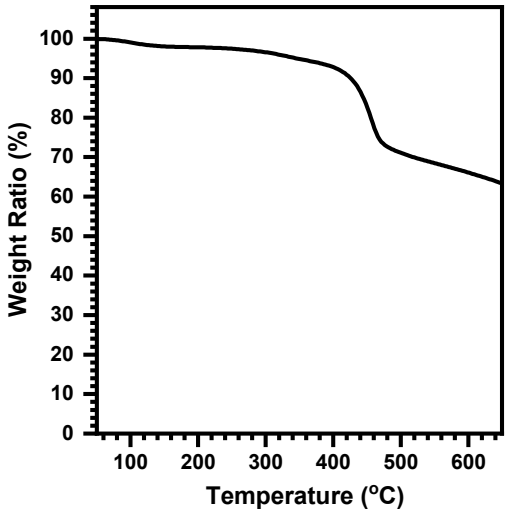

Figure S19. TGA curve of Tp-PaSO_3K-COF

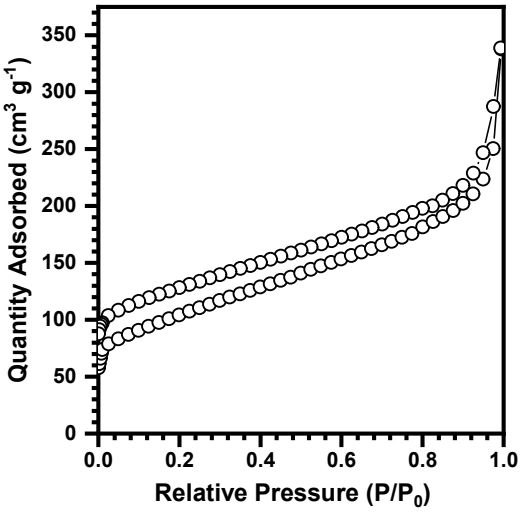

Figure S20. N_2 adsorption isotherm of Tp-PaSO_3K-COF

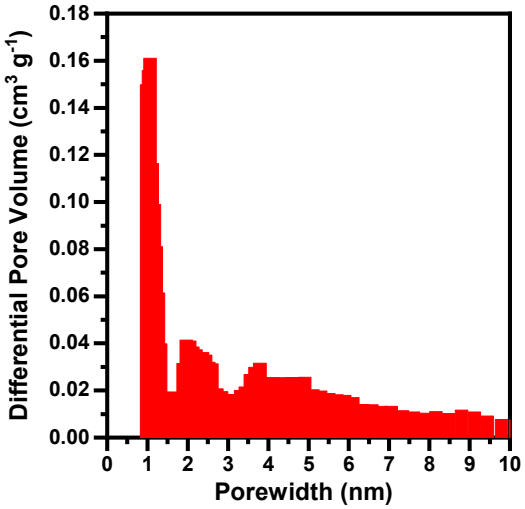

Figure S21. Pore size distribution of Tp-PaSO_3K-COF

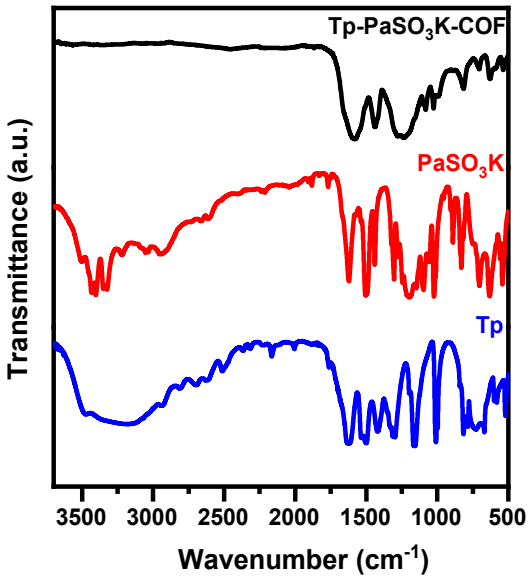

Figure S22. FT-IR spectra of Tp-$PaSO_3K$-COF, $PaSO_3K$ and Tp

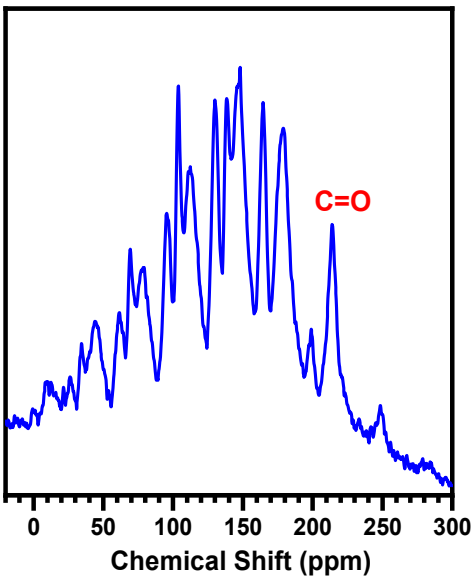

Figure S23. Solid state ^{13}C-NMR spectrum of Tp-PaSO$_3$K-COF

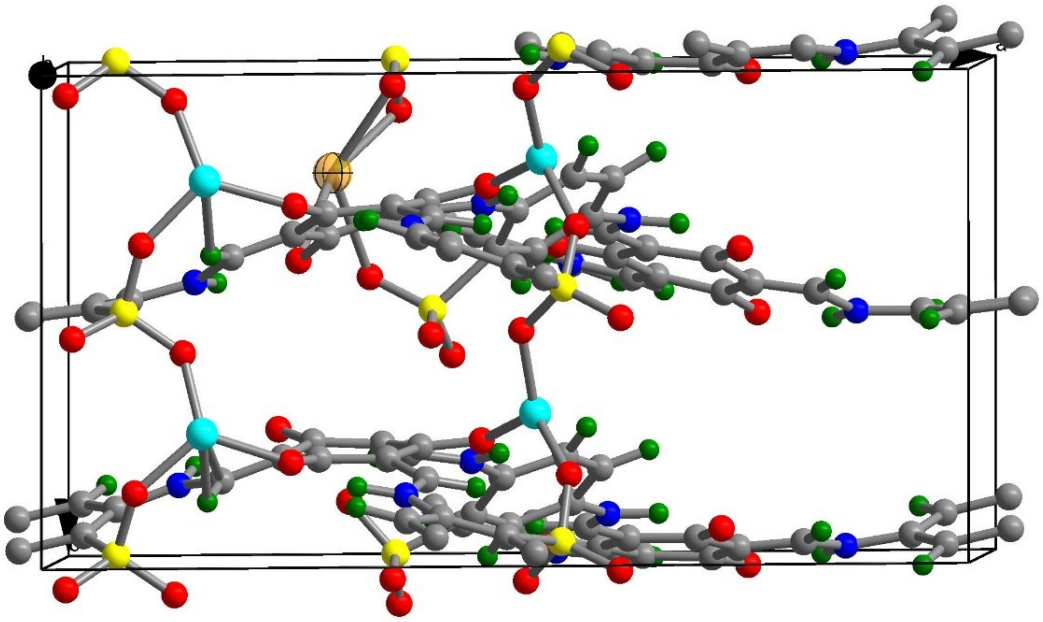

Figure S24. View of structure of initial state **1** with migration Li emphasized in large orange ball.

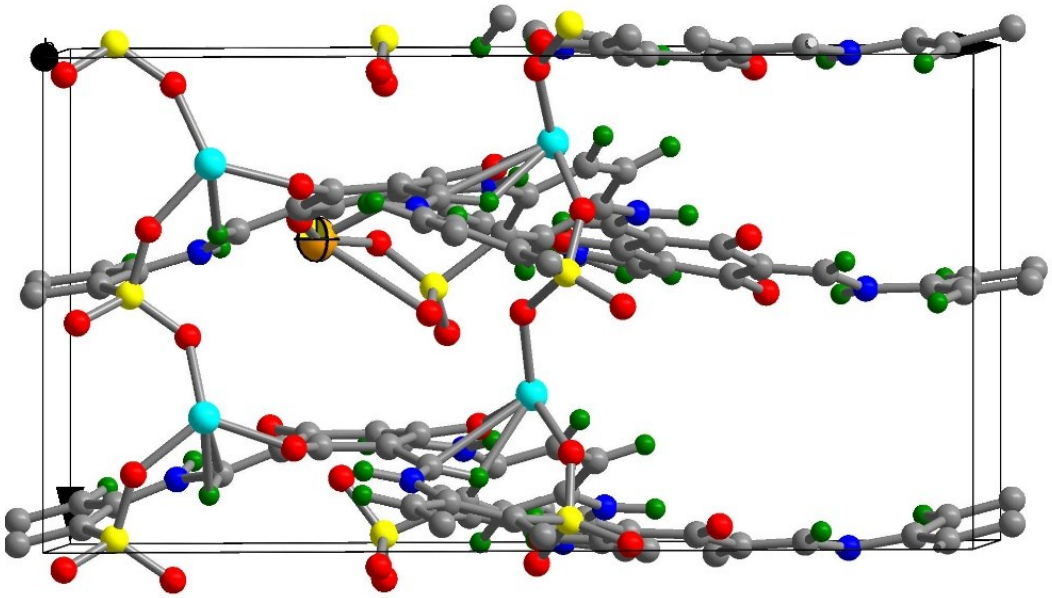

Figure S25. View of structure of transition state **1-2** with migration Li emphasized in large orange ball.

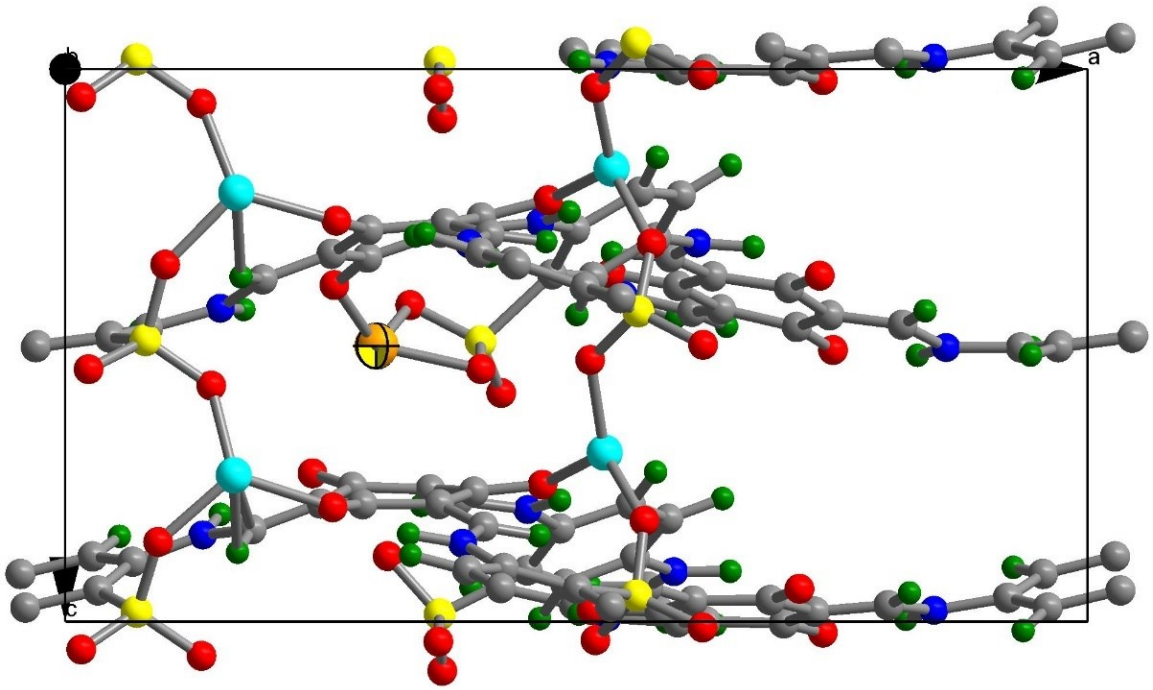

Figure S26. View of structure of intermediate state **2** with migration Li emphasized in large orange ball.

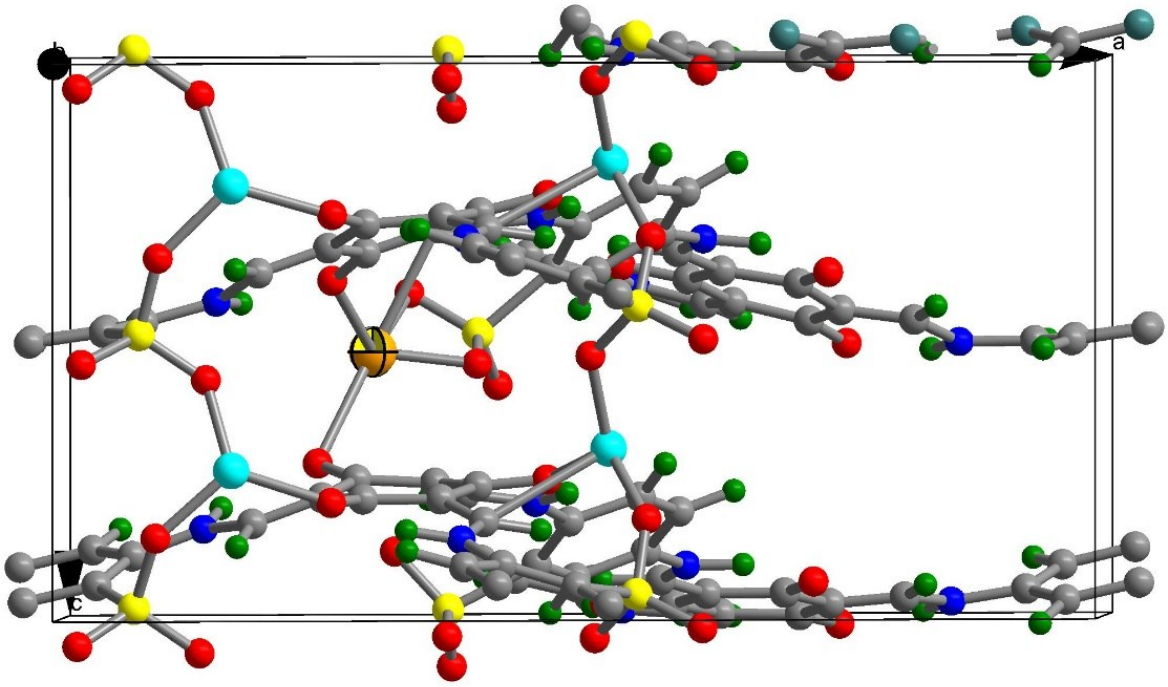

Figure S27. View of structure of transition state **2-3** with migration Li emphasized in large orange ball.

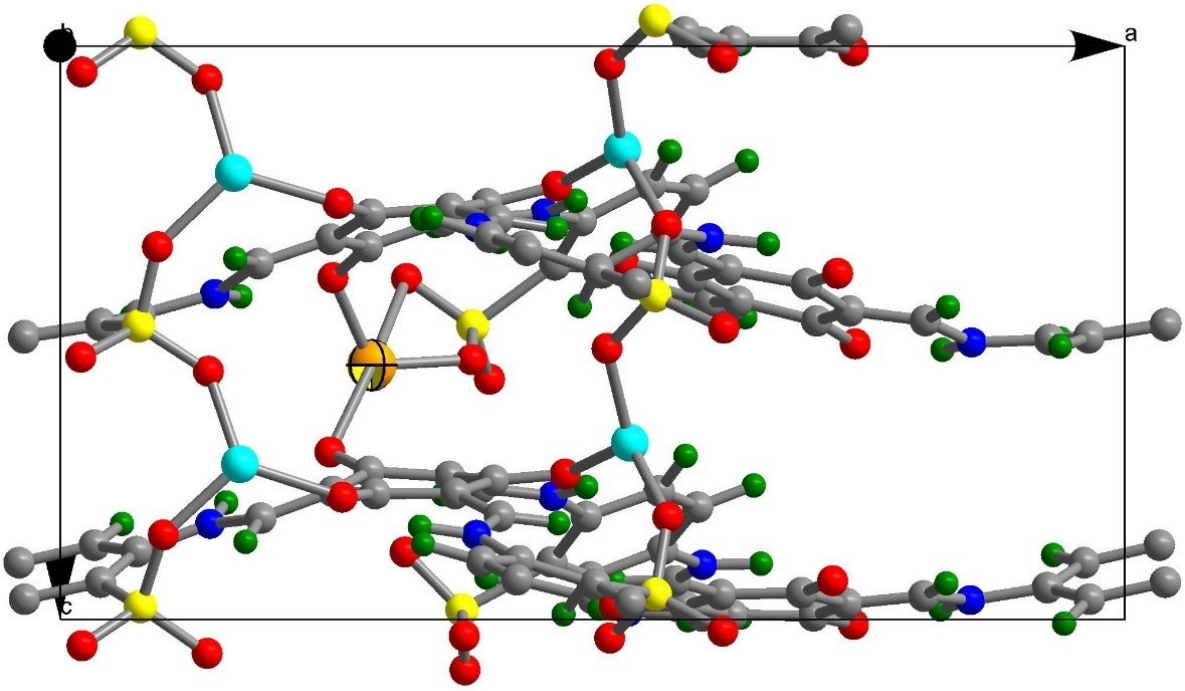

Figure S28. View of structure of intermediate state **3** with migration Li emphasized in large orange ball.

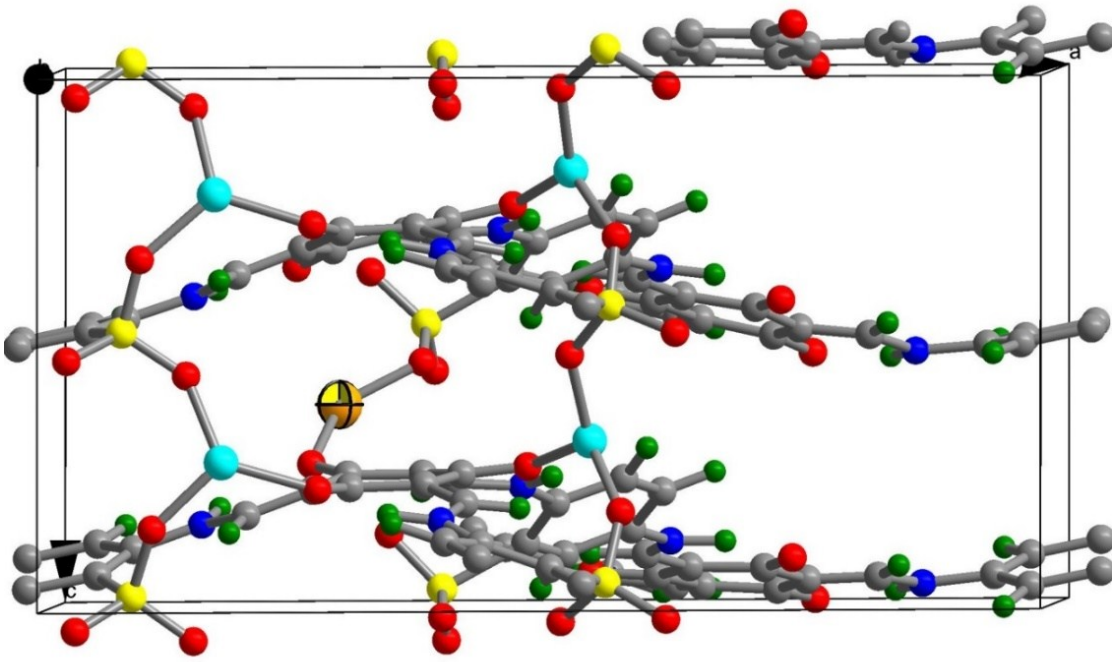

Figure S29. View of structure of transition state **3-4** with migration Li emphasized in large orange ball.

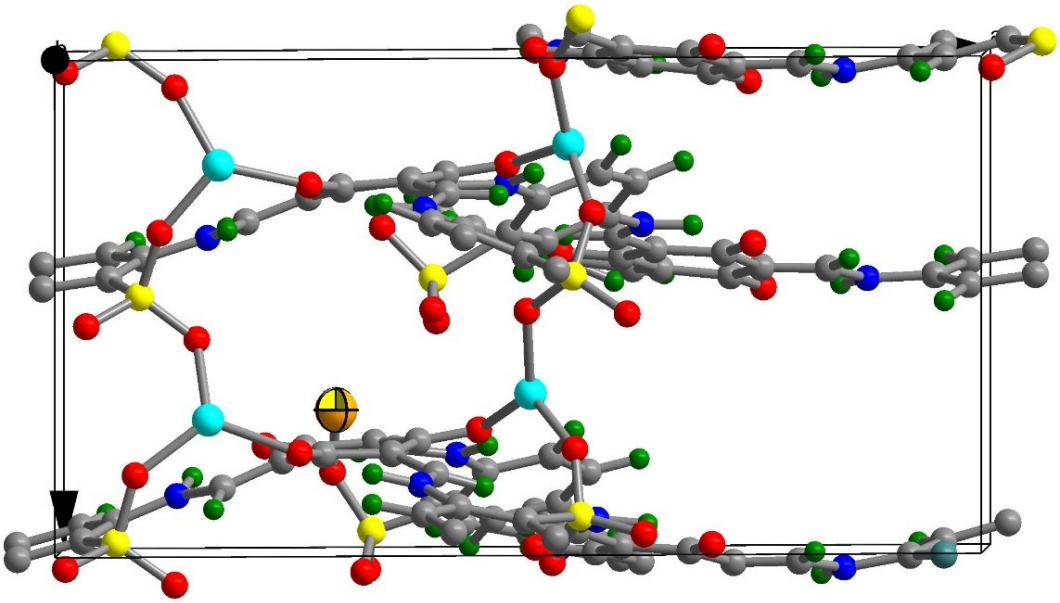

Figure S30. View of structure of final state **4** with migration Li emphasized in large orange ball.

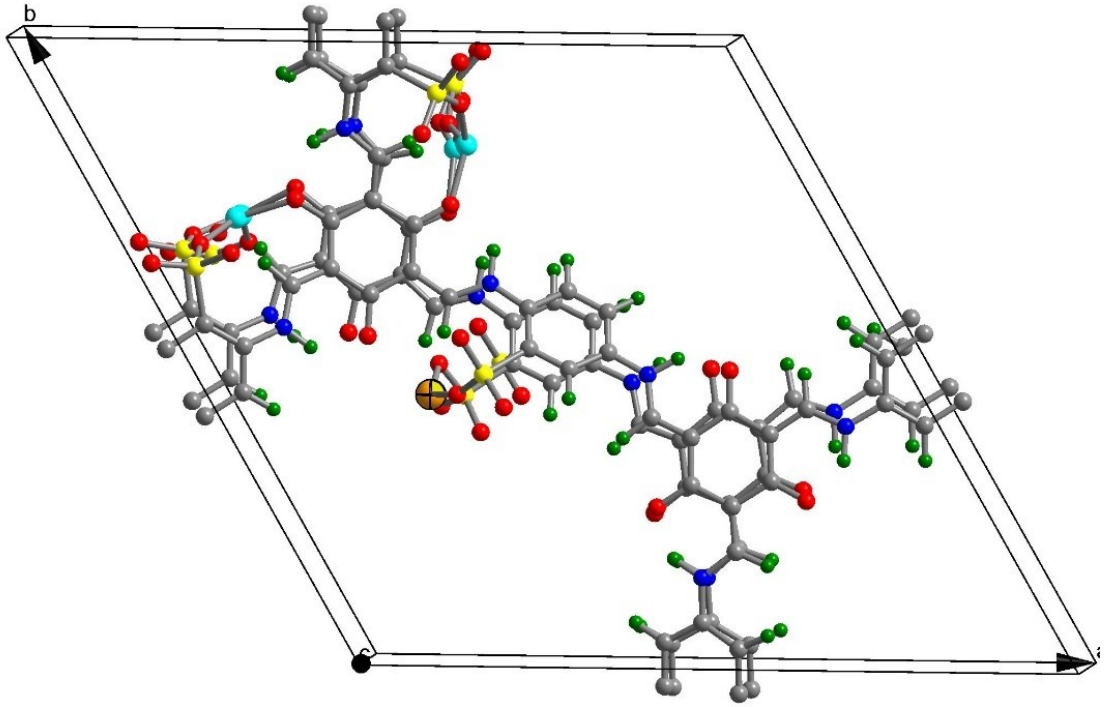

Figure S31. View of structure of transition state **4-5** with migration Li emphasized in large orange ball.

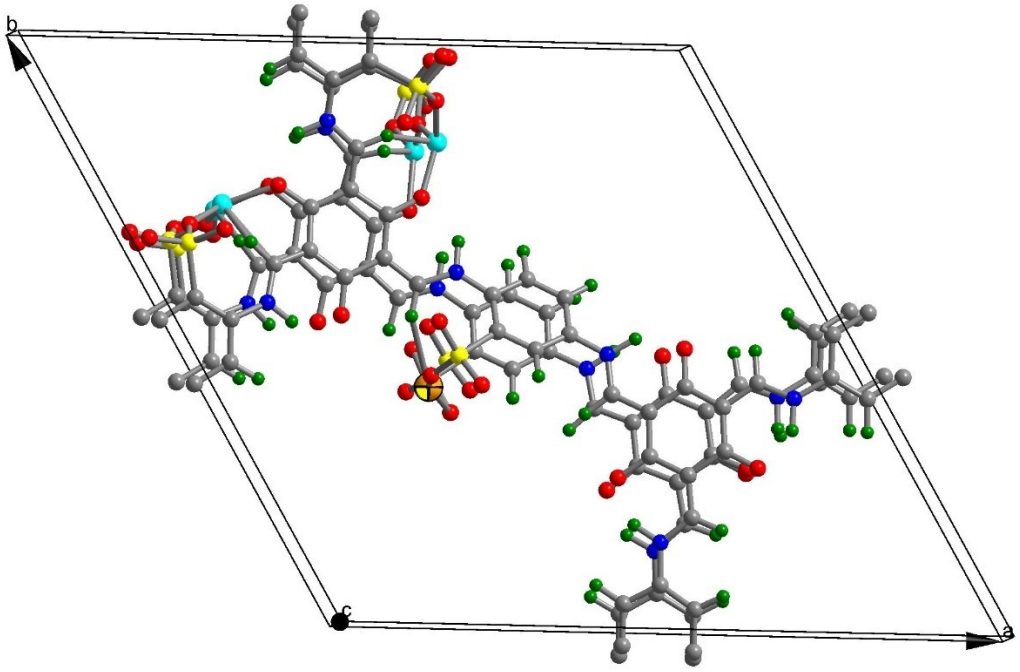

Figure S32. View of structure of intermediate state **5** with migration Li emphasized in large orange ball.

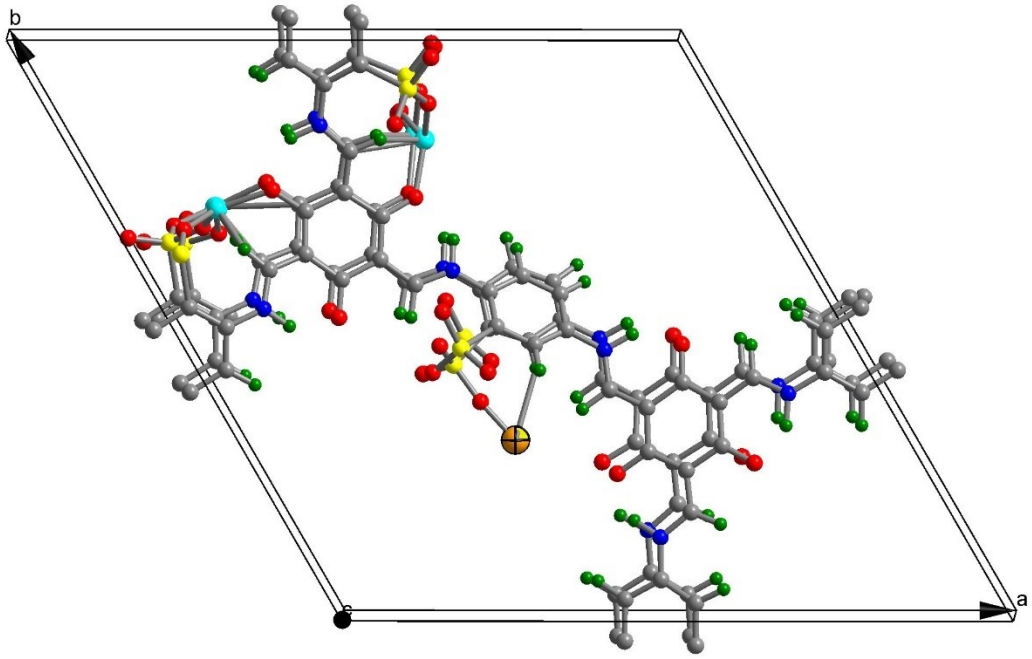

Figure S33. View of structure of transition state **5-6** with migration Li emphasized in large orange ball.

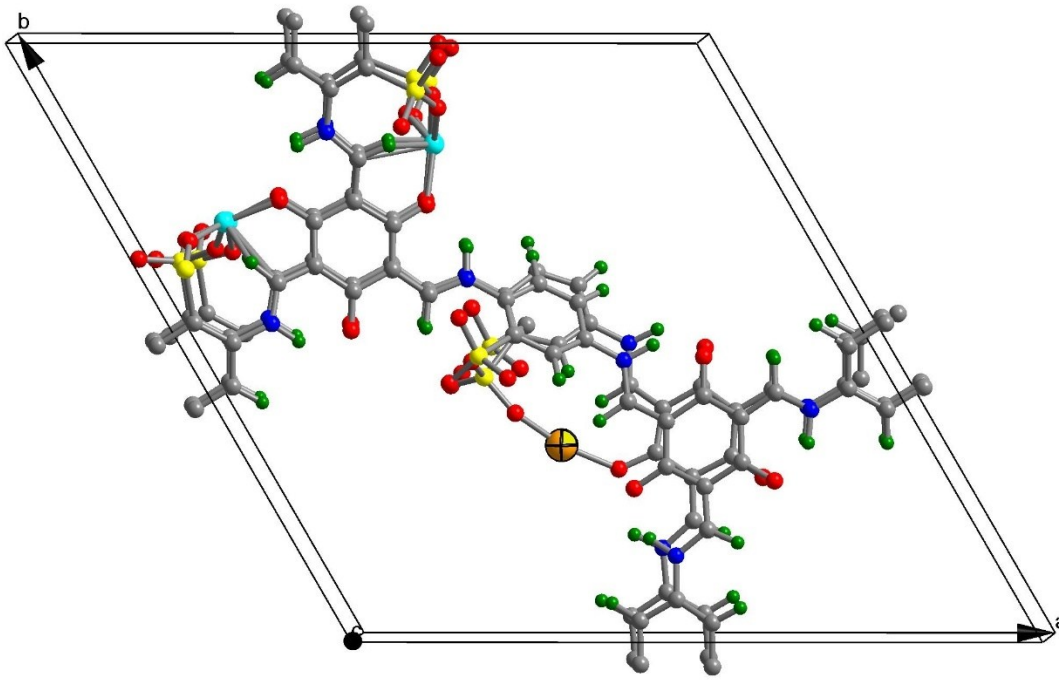

Figure S34. View of structure of intermediate state **6** with migration Li emphasized in large orange ball.

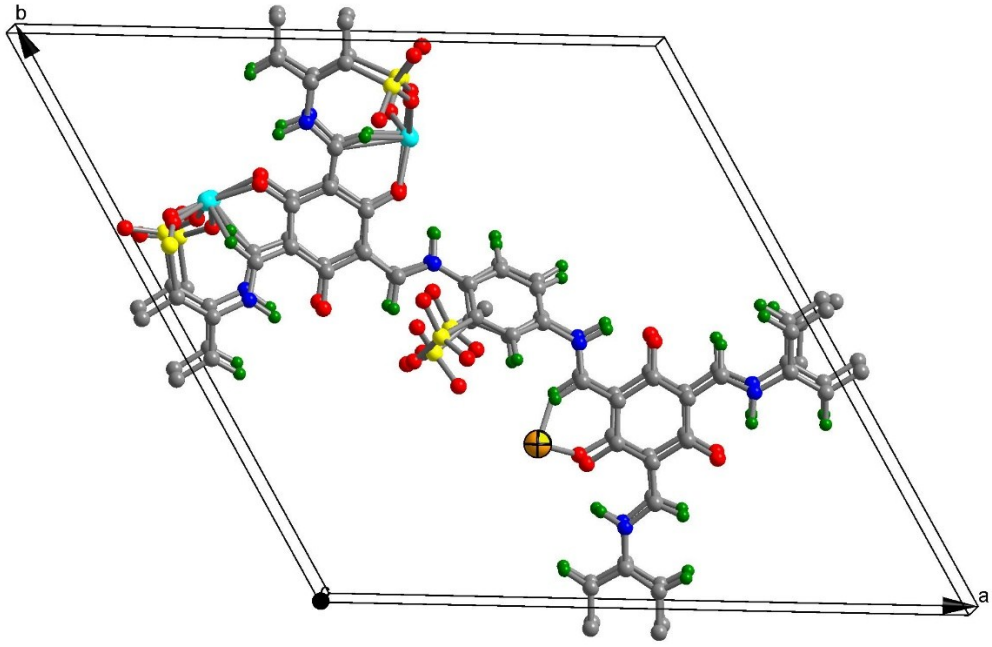

Figure S35. View of structure of transition state **6-7** with migration Li emphasized in large orange ball.

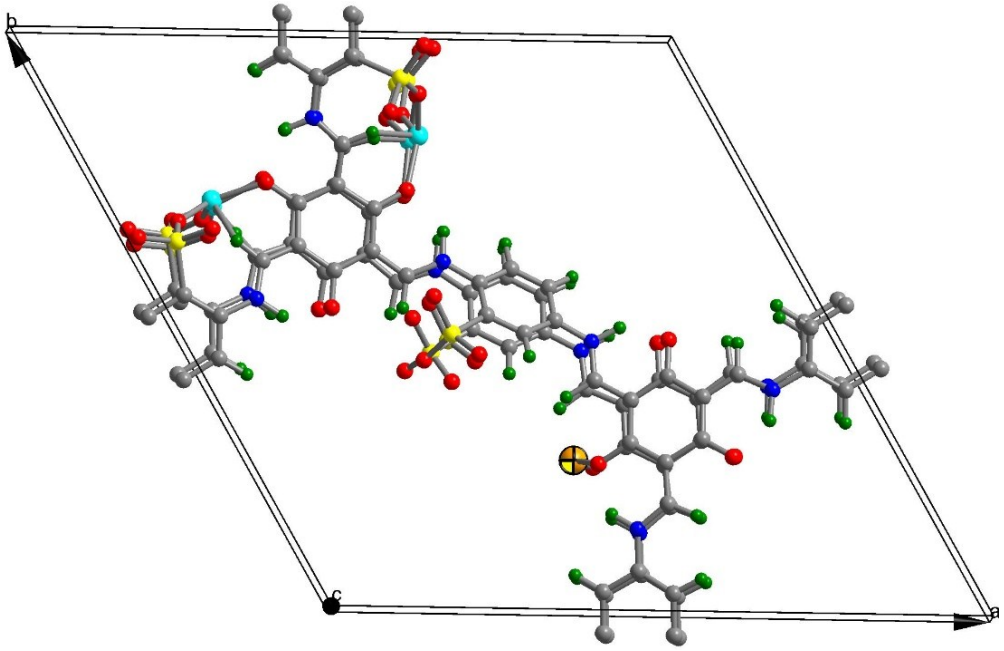

Figure S36. View of structure of state **7** with migration Li emphasized in large orange ball.

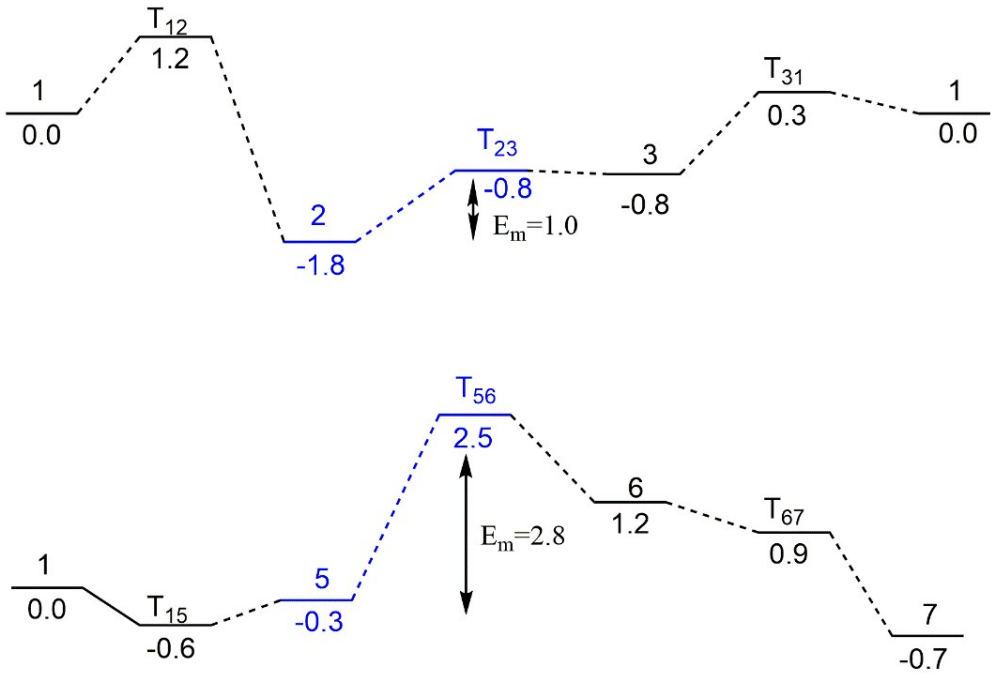

Figure S37. Reactive coordinates for axial (top) and planar (bottom) Li ion migration.

Section 5. Supporting Reference:

[S1] Aradi, B.; Hourahine, B.; Frauenheim, T., DFTB^{+}, a sparse matrix-based implementation of the DFTB method. *J. Phys. Chem. A* **2007**, *111* (26), 5678-5684.

[S2] http://www.dftb.org.

[S3] (a) Delley, B. An All-Electron Numerical Method for Solving the Local Density Functional for Polyatomic Molecules. *J. Chem. Phys.* **1990**, *92*, 508-517; (b) Delley, B. From Molecules to Solids with the DMol^{3} Approach. *J. Chem. Phys*. **2000**, *113*, 7756-7764.

[S4] Perdew, J. P.; Burke, K.; Ernzerhof, M. Generalized Gradient Approximation Made Simple. *Phys. Rev. Lett.* **1996**, *77*, 3865.

[S5] Ghosh, A.; Wang, C.; Kofinas, P., Block copolymer solid battery electrolyte with high Li-ion transference number. *J. Electrochem. Soc.* **2010,** *157* (7), A846-A849.

[S6] Kandambeth, S.; Mallick, A.; Lukose, B.; Mane, M. V.; Heine, T.; Banerjee, R., Construction of Crystalline 2D Covalent Organic Frameworks with Remarkable Chemical (Acid/Base) Stability via a Combined Reversible and Irreversible Route. *J. Am. Chem. Soc.* **2012,** *134* (48), 19524-19527.